Anatomical parameters for musculoskeletal modeling of the hand and wrist

Mirakhorlo, M; Visser, J.M.A.; Goislard de Monsabert, B.A.A.X. ; van der Helm, Frans; Maas, H.; Veeger, H.E.J.

DOI
10.1080/23335432.2016.1191373

Publication date
2016

Document Version
Final published version

Published in
International Biomechanics

International Biomechanics

ISSN: (Print) 2333-5432 (Online) Journal homepage: http://www.tandfonline.com/loi/tbbe20

Anatomical parameters for musculoskeletal modeling of the hand and wrist

Mojtaba Mirakhorlo, Judith M. A. Visser, B. A. A. X. Goislard de Monsabert, F. C. T. van der Helm, H. Maas & H. E. J. Veeger

To cite this article: Mojtaba Mirakhorlo, Judith M. A. Visser, B. A. A. X. Goislard de Monsabert, F. C. T. van der Helm, H. Maas & H. E. J. Veeger (2016) Anatomical parameters for musculoskeletal modeling of the hand and wrist, International Biomechanics, 3:1, 40-49, DOI: 10.1080/23335432.2016.1191373

To link to this article: http://dx.doi.org/10.1080/23335432.2016.1191373

INTERNATIONAL BIOMECHANICS, 2016
VOL. 3, NO. 1, 40–49
http://dx.doi.org/10.1080/23335432.2016.1191373

Taylor & Francis
Taylor & Francis Group

Anatomical parameters for musculoskeletal modeling of the hand and wrist

Mojtaba Mirakhorlo[a], Judith M. A. Visser[b], B. A. A. X. Goislard de Monsabert[c], F. C. T. van der Helm[d], H. Maas[a] and H. E. J. Veeger[a,d]

[a]Faculty of Behavioral and Movement Sciences, Move Research Institute, VU University, Amsterdam, The Netherlands; [b]Faculty of Health, Nutrition and Sport, The Hague University of Applied Sciences, The Hague, The Netherlands; [c]Department of Bioengineering, Imperial College London, London, UK; [d]Department of Biomechanical Engineering, Delft University of Technology, Delft, The Netherlands

ABSTRACT

A musculoskeletal model of the hand and wrist can provide valuable biomechanical and neurophysiological insights, relevant for clinicians and ergonomists. Currently, no consistent data-set exists comprising the full anatomy of these upper extremity parts. The aim of this study was to collect a complete anatomical data-set of the hand and wrist, including the intrinsic and extrinsic muscles. One right lower arm, taken from a fresh frozen female specimen, was studied. Geometrical data for muscles and joints were digitized using a 3D optical tracking system. For each muscle, optimal fiber length and physiological cross-sectional area were assessed based on muscle belly mass, fiber length, and sarcomere length. A brief description of model, in which these data were imported as input, is also provided. Anatomical data including muscle morphology and joint axes (48 muscles and 24 joints) and mechanical representations of the hand are presented. After incorporating anatomical data in the presented model, a good consistency was found between outcomes of the model and the previous experimental studies.

ARTICLE HISTORY
Received 12 June 2015
Accepted 12 April 2016

KEYWORDS
Musculoskeletal modeling; intrinsic muscles; extrinsic muscles; extensor mechanism

Introduction

Modeling of the human hand can reveal important information about biomechanical mechanisms and provide a basis for investigating hand dysfunction and pathologies. Building a complete musculoskeletal model of the hand is highly complicated due to its intricate anatomy, including the intrinsic muscles and the extensor mechanism, and the high number of degrees of freedom (DOF).

Hand function results from the combined contribution of intrinsic and extrinsic muscles. Extrinsic hand muscles originate from the forearm with a long tendon inserting onto the (meta) carpals or fingers. The origins of intrinsic muscles can be found distal to the wrist joint. They insert onto either extensor mechanism or fingers. The extrinsic muscles are thought to be the main force producing muscles, while the intrinsic muscles appear to work as modulators for balancing the moments around finger joints (Buford et al. 2005). The extensor mechanism of the fingers is a collagenous web in which the Extensor Digitorum Communis muscle (EDC) and the intrinsic muscles are integrated, and which allows for force transfer from the intrinsic muscles at the metacarpal phalangeal (MCP) joint to the extensor side of the fingers (Levangie & Norkin 2011).

Several models of the hand and fingers have been published. Chao et al. (1976) reported a detailed investigation into the musculoskeletal mechanics of only the fingers including estimated force data. An et al. (1979) developed a complete hand model, based on the anatomical data of 10 cadaveric specimens. While very extensive and a major step forward, the model was still limited in the sense that it only included orientation and location of the muscles and tendons and lacked morphological parameters of muscles. A model including the shoulder, elbow, and hand was presented by Holzbaur et al. (2006) but this model did not include the intrinsic musculature of the hand. Due to aforementioned complexities of modeling of whole hand, several other models have focused on parts of the hand such as the thumb (Valero-Cuevas et al. 2003; Vigouroux et al. 2009; Wu et al. 2009) or separate fingers (Brook et al. 1995; Valero-Cuevas et al. 2000; Sancho-Bru et al. 2001; Wu et al. 2010). Recently more complete models are introduced (Sancho-Bru et al. 2014; Vignais & Marin 2014) however a limitation to these studies is that they collected data from various resources and input to their models. Anatomical data, such as muscle architecture, serve as the basis for these biomechanical models of the hand. In some cases, input data such as muscle architecture were taken from

CONTACT Mojtaba Mirakhorlo m.mirakhorlo@vu.nl
The supplementary material for this paper is available online at http://dx.doi.org/10.1080/23335432.2016.1191373

previous studies and were scaled to be incorporated in the model assuming that anatomical parameters are correlated. Holzbaur et al. (2007) showed a consistent distribution of muscles among subjects for muscle volume and PCSA. However, this assumption may lead to model inaccuracy since this correlation cannot be applied to all parameters (for instance variability in muscle length was relatively high in Holzbaur's study). It also should be noted that Holzbaur et al. (2007) investigated only extrinsic muscles of hand. Their approach might not be justified for intrinsic muscles because it has been shown that there is greater diversity (in muscle mass, belly length, and length) among intrinsic muscles in comparison with extrinsic muscles (Jacobson et al. 1992). Furthermore, some other anatomical data that are needed as inputs to models, such as the muscle origins and insertions, are not available in the previous literature. In a optimized base approach, not with dissection, Lee et al. (2015) calculated muscle attachment points for fingers using a model built in OpenSim. They optimized these points to fit in the experimental moment arms of the muscles.

Currently, no complete anatomical data-set of musculature of the hand has been published. The purpose of this study was to collect the morphological parameters necessary for constructing a complete model of the human hand and wrist. A general musculoskeletal model of the hand is presented on which the choices on the level of detail required for the anatomical data collection were based.

Methods and results

The procedure for measuring and computing hand musculoskeletal data comprises four main steps (Figure 1): measuring basic anthropometric data, digitization of the hand geometry, kinematic estimation of joint geometry, and the measurement of muscle properties.

Model description

We developed a linked segment model of the hand in SPACAR via a similar approach to the Delft Shoulder and Elbow Model (DSEM) (van der Helm 1994; Asadi Nikooyan et al. 2011) which can be driven kinematically. The model consists of 22 rigid bodies, the carpal bones were modeled as a single body, each of the other bones in the hand and forearm have been modeled as individual rigid bodies (Figure 2). The model has 27 degrees of freedom (DOF) at the joints, and 46 muscles. Muscles and tendons are modeled either as straight-line elements between two points or as curved elements that can wrap around a joint surface such as for the finger extensors.

The long poly-articular muscles, more specifically the extrinsic finger flexors and extensors, are divided in multiple muscle elements each crossing one joint which all bear the same force, neglecting intermuscular and intertendinous connections. The most proximal muscle part represents the muscle belly and allows active contraction

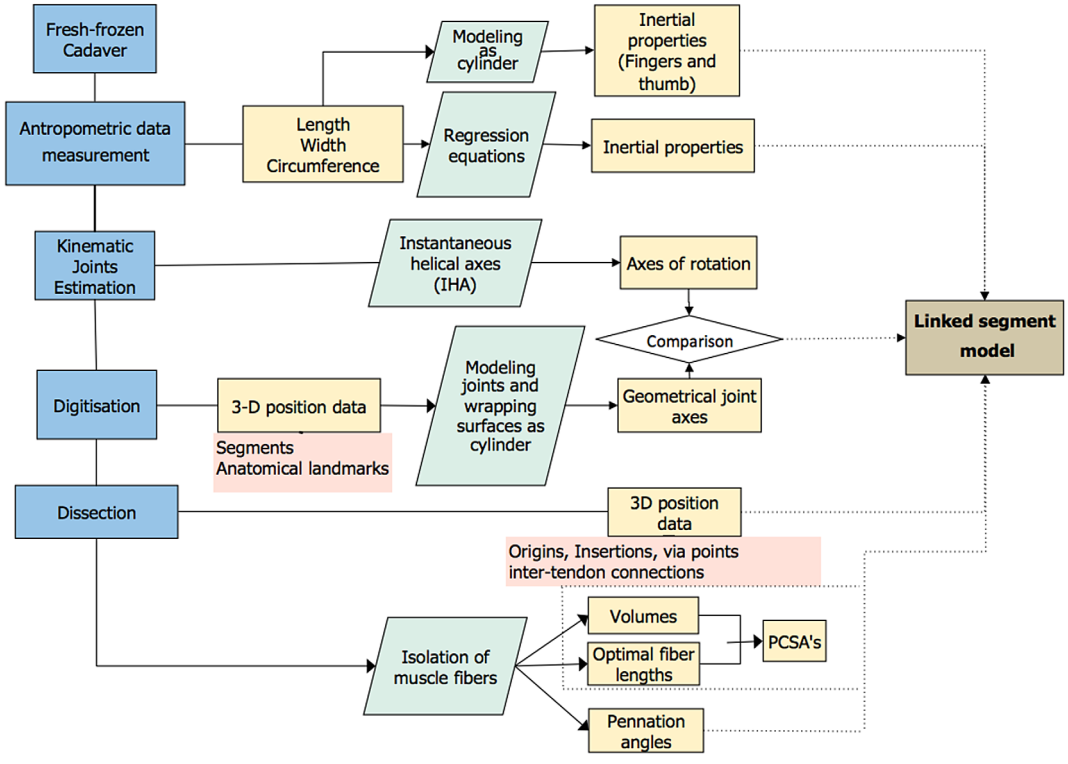

Figure 1. Flow chart of the experimental procedure.

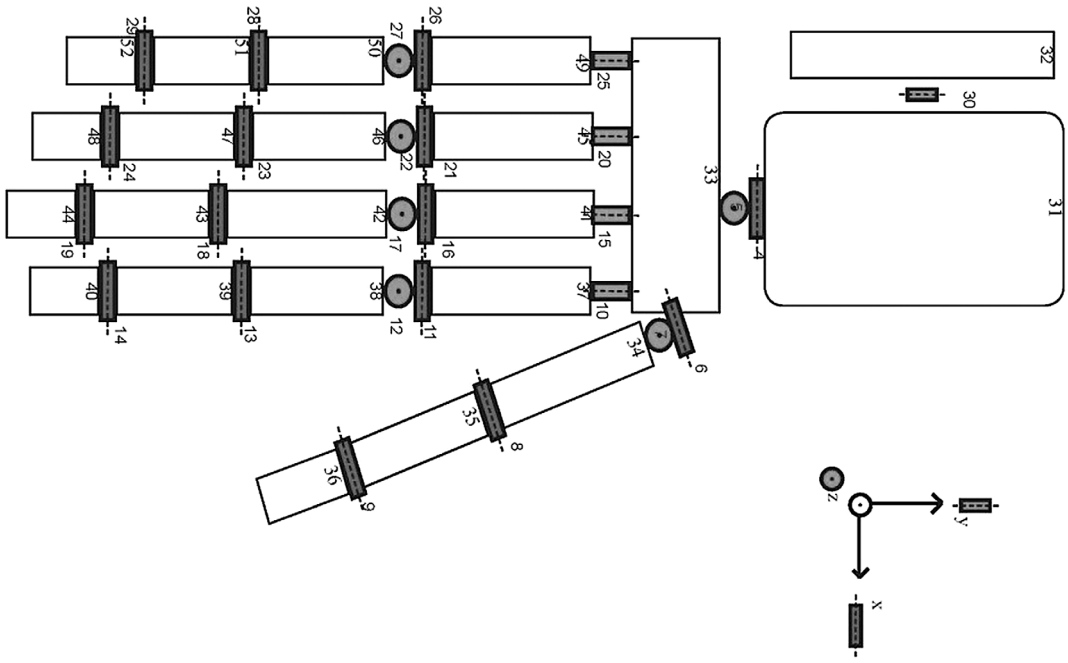

Figure 2. Mechanical linked segment model of the hand, white blocks present the multi-node segments. Red, green, and blue elements represent flexion-extension, *ab*-adduction, and axial rotation axes.

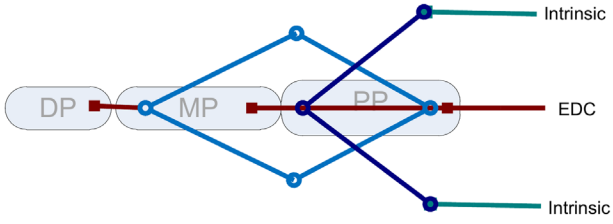

Figure 3. Model structure of the extensor web with the Extensor Digitorum muscle and intrinsic muscles included. The bullets and squares represent the insertion- and via-points included in the model. DP = Distal Phalange. MP = Medial Phalange. PP = Proximal Phalange.

(active force of muscle is calculated based on a hill-type model for muscle (Hill 1938)); the distal elements represent the long tendons, which are modeled by a constant length neglecting their elastic properties. Muscles and tendons are connected with 'via points' that are allowed to move distally as the finger flexes and proximally as the finger extends (Figure 3). This will result in a change of muscle fiber length, while the total length of the tendon elements remains constant. Forces are equal to each other in 'via points' with two elements; hence, forces exerted to the rigid body will also be the same. At 'via points' with lateral connections, the forces of the distal elements are equal to the combination of forces of proximal elements. Consequently, force exerted on a proximal segment will be equal to the force on the distal element.

Anatomical data collection

Data were obtained through dissection and digitization of a right arm from a fresh-frozen cadaver (Female, 87 years old). A 3D position tracking system (Optotrak Certus, NDI, RMS error calibration < 0.36 mm) was used to collect 3-D orientation and position data of the segments, anatomical landmarks, and muscles. Two 3-camera units were positioned around the specimen pointed at a viewing angle of approximately 80° and data were collected at a sample frequency of 75 Hz. The landmarks and muscle points (origins, insertions, and via points for long muscles) were digitized using a 6-marker pointer with a metal tip, the transformation of the pointer markers for calculating the endpoint position of the pointer resulted in an error < 0.45 mm. The pointer was rotated while its endpoint was rigidly fixed. The spheres were estimated on the markers locations. The averaged center of all markers was considered as the endpoint of the pointer and the deviation as the actual error (0.45 mm). A list of abbreviation is provided in the table 1 of supplementary material (Table S1).

Inertial parameters

Before dissection, anthropometric data (segment length, width, and circumference) of forearm and fingers were measured (Table S2). Inertial properties of segments – hand and forearm – were estimated using regression equations based on the work by Zatsiorsky et al. (1990). Inertial properties of fingers and thumb segments were

Table 1. Inertial properties calculated from anthropometric data based on Zatsiorsky et al. 1990) (forearm and complete hand), from anatomical landmarks using standard cylindrical inertial properties (MC1 to DP5). Data not estimated for DP2 due to missing landmark. Coordinates of Center of mass ($CoM_{x,y,z}$) are calculated relative to ulnar styloid. CoM is relative to proximal of segment.

Segment	Mass (g)	CoM_x (mm)	CoM_y (mm)	CoM_z (mm)	CoM (mm)	I_z (mm²*g)	I_x (mm²*g)	I_y (mm²*g)
MC1	18.55	71.08	−42.11	−8.64	22.23	3670.68	1231.26	1231.26
PP1	8.75	87.05	−73.02	0.99	13.92	783.72	437.68	437.68
DP1	10.08	99.06	−99.24	1.91	16.04	1116.60	504.37	504.37
PP2	13.31	51.51	−109.73	8.18	22.39	2538.93	630.12	630.12
MP2	6.74	45.29	−143.67	6.02	12.41	491.56	291.40	291.40
DP2	*x*	*x*	*x*	*x*	*x*	*x*	*x*	*x*
PP3	14.96	28.81	−109.22	4.65	27.66	4136.94	644.11	644.11
MP3	6.41	22.25	−148.30	−7.79	14.30	551.21	228.85	228.85
DP3	5.84	20.89	−170.23	−23.58	13.03	434.72	208.53	208.53
PP4	9.91	0.62	−100.61	6.52	22.38	1828.09	348.95	348.95
MP4	5.77	−6.53	−137.14	1.32	15.85	567.28	167.42	167.42
DP4	4.83	−5.78	−164.50	−8.23	13.25	352.76	140.00	140.00
PP5	6.50	−12.14	−91.16	3.17	19.97	947.90	168.22	168.22
MP5	3.49	−19.10	−121.99	−1.49	12.45	219.69	78.02	78.02
DP5	2.66	−19.13	−141.74	−9.28	9.46	108.90	59.28	59.28
Total mass fingers	118							
Hand (complete)	450				119.73	13.773 (cm²*kg)	10.364 (cm²*kg)	5.424 (cm²*kg)
Palm (hand-fingers)	332							
Forearm1	933				143.52	50.082 (cm²*kg)	46.774 (cm²*kg)	8.597 (cm²*kg)

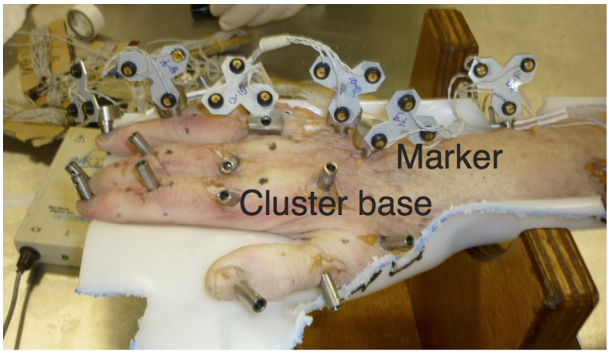

Figure 4. Specimen in reference position with cluster bases fixated to all segments, marker clusters attached to the ring finger, MCIII, and ulna.

estimated as cylinders. Related diameters were obtained from bony landmarks.

Twenty-two rigid cluster bases were rigidly attached to the following bone segments: humerus, ulna, radius, MCP-I to MCP-V, PP-I to PP-V, MP-II to MP-IV, and DP-I to DP-V (Figure 4). The cluster bases remained in place until all data were collected. The cluster bases were firmly attached to the underlying bone such that the marker clusters could be easily clicked onto these bases in a repeatable pose. The bases were fixed to the bones using self-tapping wood screws. The bases also presented four sharp 'teeth' at their base, which partially penetrated the bone cortexes, therefore preventing any rotation along their longitudinal axis. To click the clusters in their respective bases, a ball and spring plunger was used. Seven click-on marker clusters with three tracking markers were used to track the segments during digitization. Radius, ulna, and MCPIII clusters were always equipped during the experiment and used as local references for further processing. After marker cluster placement, the specimen was held in a natural resting position, in a custom made cast in which all marker clusters would be visible to the tracking system (Figure 4). In a series of reference measurements, the poses of the marker clusters, as well as the coordinates of relevant anatomical landmarks were recorded for all segments. All subsequent data recordings were rotated and translated back to the original resting position of the specimen using the segment marker cluster poses. For all transformations to the resting position, the error, which was calculated by the method proposed by Söderkvist and Wedin (1993) was smaller than 0.15 mm.

All data were described in the coordinate frame of the ulna, with the ulnar styloid (US) as the origin and the following axes:

- Y: the line from US pointing to the midpoint of the line between the medial (EM) and lateral epicondyle (EL) of the humerus
- Z: perpendicular to Y and the line from US to the radial styloid (RS)
- X: perpendicular to Y and Z, pointing radially.

Geometry: joint axes and surfaces

For each of the joints, uni-axial motion data were collected by passively moving each of the joints through their full range of motion whilst collecting the segment marker data using the tracking system. The measurements were taken prior to muscle dissection, when the muscles, tendons, and skin were still intact. From these data, the kinematic

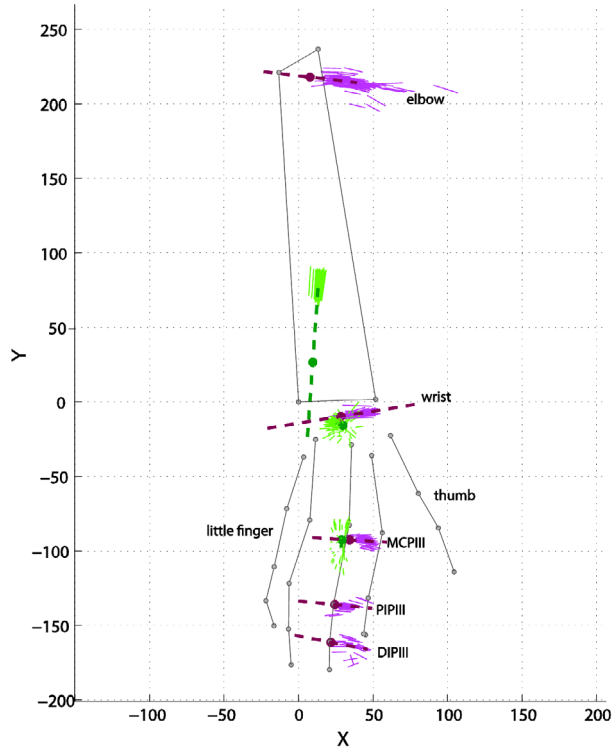

Figure 5. IHA and estimated joint axis for the middle finger. Green solid lines: instantaneous abduction-adduction and pro-supination axis, purple solid lines: instantaneous flexion axis. Dashed lines, estimated joint axes. Dorsal view of the hand and forearm.

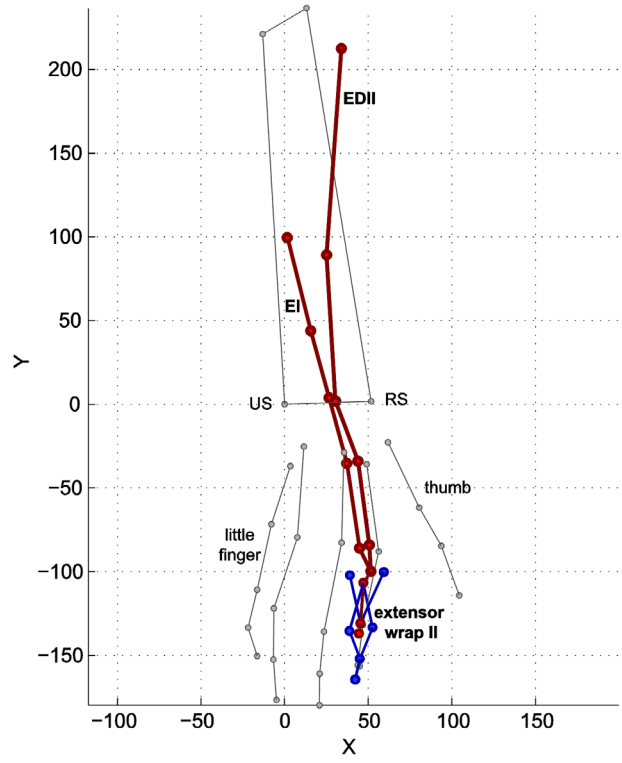

Figure 6. Palpated data points for the EDCII, EI, and extensor web with the main anatomical landmarks (grey). Dorsal view. EDCII = Extensor Digitorum Communis of second finger EI = Extensor Indicis.

axes of rotation were estimated using the instantaneous helical axis (IHA) method (Veeger et al. 1997). From the kinematic axes, the joint poses were described with the optimal direction vector and a pivot point on that vector. IHAs for the whole range of motion and mean joint axes for the middle finger, wrist, and elbow are illustrated in Figure 5. Averaged direction vectors and their related pivot points for all the joints were provided in Table S3. Cylinders were fitted through digitized finger joint surfaces (actual procedure for fitting explained in the next section) for hinge joints. Differences between axes of these cylinders, which can be considered as geometrically joint axes, and kinematically derived axes were provided in Table S3. The differences between some axes were relatively high (for instance PIPV and MCPII). Unfortunately, we could not find other studies that explicitly published data on joint axes to compare with our results***. However by inspecting the axes visually (Figure 6s), IHA axes appeared to be a more appropriate indicator of joint axes. Vectors calculated using IHA method incorporated to the model.

Geometry: bony landmarks, muscle origins, insertions, via points, and geometrical shapes

The 3D positions of 48 bony landmarks were digitized and are listed in the supplementary material (Table S4). Once all landmarks were digitized, the procedures were repeated for a selection of the landmarks of three fingers: middle, ring, and little (14 landmarks) in order to examine the intra-observer reliability. The mean difference for the 14 repeated landmarks was 2.6 mm (SD 1.9) (Table S5).

After recording bony landmarks, the arm was dissected and muscle attachment points, via points, and joint surfaces were digitized, always relative to their relevant marker cluster (allowing for subsequent transformation back to the resting position). The extrinsic finger muscles with a common muscle belly and multiple distal tendons (FDP, FDS, EDC) were dissected in separate muscle heads for each finger by visual identification of the muscle fibers belonging to each tendon. Muscles were freed from their underlying structures, leaving the attachment sites intact. For each of the muscles, the origin, insertion, via points over the joints, and inter-tendon connections were identified and digitized. As an example, palpated data points for the EDC, EI (Extensor Indicis), and extensor web of index finger are shown in Figure 6. After removal of the muscles and inter-tendon connections, the thumb and finger joint surfaces were digitized from the extensor side. For each joint surface a cylindrical shape was fitted on the data points using a Levenberg–Marquardt optimization. The parameters for the estimated cylindrical curves

are presented in the supplementary material (Table S6). During the dissection, the specimen was kept moist with saline solution.

The 3D position data of insertions, origins, and via points for the muscles are listed in the supplementary material (Table S7). Table S7 also includes muscle position data for the extensor wrap points. Supplementary figures of 1 to 5 illustrate these wrapping points in the extensor web of each finger.

Muscle morphological parameters

After digitization, muscles were dissected free from the specimen, pinned to a wooden board, and fixed in a formalin solution (4%), to obtain muscle architecture parameters at a later stage.

After fixation, for each muscle, tendon length and fiber length were measured using digital callipers. The pennation angle was defined as the angle between the muscle fiber direction and the muscle line of action. Pennation angle was measured only for pennation angles larger than 10. The muscle was weighed on a digital scale with 0.1 g accuracy after removing tendon, fat, and connective tissues. Using the laser diffraction method (Borst et al. 2011), sarcomere length was measured at a proximal, middle, and distal location along the length of each fiber and subsequently averaged to obtain a mean sarcomere length.

Optimum fiber length was calculated by dividing the fiber length by mean sarcomere length and multiplication with the optimal fiber length of 2.7 µm (Walker & Schrodt 1974). For each muscle, the physiological cross-sectional area (PCSA) was calculated by the following equation:

$$PCSA\left(mm^2\right) = \frac{mass(g)}{density\left(\frac{g}{mm^3}\right) \cdot optimum\ fiber\ length\ (mm)} \quad (1)$$

As in previous work (Borst et al. 2011), a muscle density of 0.0010567 g/mm^3 was assumed. Table 2 presents the muscle morphology data for all of the digitized muscles. The belly of FDSII consisted of two bellies arranged in series. For each of these bellies, fiber length and pennation angle were assessed. The mass and tendon length were measured for the whole muscle because in the model both muscle bellies will be represented as one. The fiber lengths of these two bellies were summed and their pennation angles were averaged to allow a single FDSII model input.

Special cases

For the EDC an anatomical variation was observed: EDC only branched to the index, middle, and ring finger but had no tendon to the little finger. The extensor web of the little finger was mainly originating from ED min. ED min had two branches: the main branch to the little finger and a smaller one to the ring finger.

Model output

To assess to what extent measured data are accurate and if the model works properly, some model evaluations were conducted. Changes in total length (excursion) of extrinsic and intrinsic muscles during flexion of the index finger MCP joint were computed and compared with experimental data from An et al. (An et al. 1983) (Figure 7).

Discussion

This study presents an extensive data-set including segment inertia, muscle and joint geometry, and muscle morphology needed for musculoskeletal modeling of the human hand and wrist. The schematic of the model of hand and wrist, which we will construct using these anatomical data was also provided. The model is based on the Delft shoulder and elbow model (Asadi Nikooyan et al. 2011) and includes all the extrinsic and intrinsic muscles of the hand taking into account the extensor mechanism of the fingers. Based on our knowledge this is first comprehensive model of hand and wrist, which comprises the extensor mechanism and intrinsic muscles of the hand.

To our knowledge, there are no other data-sets to compare with anatomical data measured in this study. To investigate the validity of some measured parameters such as muscle attachment points and joint positions, muscle excursions were compared with experimental data. Model outputs for the extrinsic muscles were quite comparable with those of An et al. (An et al. 1983) as it was shown in Figure 7. The small differences may be explained by different body anthropometrics. Differences between excursions for intrinsic muscles were higher in terms of magnitude, but with comparable patterns. In general, results indicated that the implemented anatomical data were realistic, both for intrinsic as well as extrinsic muscles.

There are some limitations to our study. The tendons were assumed to be rigid neglecting their elastic properties. This simplification will probably have effect on model output to a limited degree since finger flexors have been shown to experience small amounts of strain under normal loads (Ward et al. 2006). With regard to the hand inertial properties, finger segments were estimated as solid cylinders. It seems to be a reasonable assumption and has been used before to calculate these parameters (Friedman & Flash 2009).

The specimen dissected in this study was old and might, despite careful selection based on visual inspection, have suffered from some musculoskeletal disorder, affecting

Table 2. Muscle morphological parameters including the segment of origin and insertion and the number of via points. The geometrical data can be found in the supplementary material. *These figures are for both fourth and fifth fingers together. **Proximal and distal together. ***Together with Extensor Digiti Minimi

Muscle	Number of via points	Origin	Insertion	Optimum Fiber Length (mm)	Tendon length (mm)	Pennation angle (deg)	Mass (g)	PCSA (mm^2)
Wrist								
Extensor Carpi Radialis Longus	1	Hum/Rad	MC2	72.7	210	0	13.9	181.1
Extensor Carpi Radialis Brevis	1	Hum/rad	MC3	35.1	185	12	9.6	258.5
Extensor Carpi Ulnaris	1	Hum/Uln	MC5	45.6	137	11	8.9	184.8
Flexor Carpi Radialis	1	Humerus	MC2	76.4	188	0	7.4	91.6
Flexor Capri Ulnaris	1	Hum/uln	MC3,MC5	72.8	200	10	13.3	173.0
Palmaris Longus	1	Hum/Uln	MC3	89.2	247	0	3.4	36.1
Palmaris Brevis	X	Not present		*x*	*x*	*x*	*x*	*x*
Pronator Teres	0	Humerus	Radius	38.1	92	0	9.5	236.3
Pronator Quadratus	0	Ulna	Radius	29.9	7	0	5.5	173.8
Supinator	0	Humerus	Radius	26.6	77	40	10	355.2
THUMB								
Abductor Pollicis Longus	2	Ulna	MCl	50.1	156	12	5.9	111.4
Extensor Pollicis Longus	1	Ulna	ExtWrap	44.0	202	0	2.9	62.3
Extensor Pollicics Brevis	2	Ulna	ExtWrap	40.5	145.7	21	2.5	58.4
Opponens Pollicis	0	MC3	MC1	29.9	255	0	3.7	117.1
Adductor Pollicis Oblique	0	MC3	PP1	30.7	0	0	4.2	129.3
Adductor Pollicis Transverse	0	MC3	PP1	40.8	24	24	2.3	53.3
Flexor Pollicis Brevis ssuperficialis	0	MC3	PP1	49.6	14,8 7,1	0	1.1	21.0
Flexor Pollicis Brevis deep	0	MC3	PP1	23.0	12	0	0.4	16.5
Flexor Pollicis Longus	3	Radius	DP1	59.0	258	20	7.8	125.2
Abductor Pollicis Brevis	0	MC3	PP1	49.7	24.5	0	2.3	43.8
IOPI	*x*	Not present		*x*	*x*	*x*	*x*	*x*
INDEX finger								
Extensor Indicis		Ulna	ExtWrap	45.0	206	0	2.9	61.0
Extensor Digitorum II	1	Ulna		42.6	153	0	2.2	48.9
Flexor Digitorum Superficialis II							29.1	
FDSIIprox	5	Hum/Ulna	MP2	52.1	215**	16	10.1**	183.6
FDSIIdist		Extra belly FDSII		34.9	215**	12	10.1**	
Flexor Digitorum Profundus II	7	Ulna/ radius	DP2	90.9	260	10	13.3	138.5
Lumbricales I		FDP2/MP2	ExtWrap	78.4			0.6	7.2
Palmar Interosseus II	1	MC2/MC3	PP2	25.6	25	0	1.4	51.7
Dorsal Interosseus 1MC1	1	MC1	PP2	39.6	10.5	15	2.6	62.1
Dorsal Interosseus 1MC2	1	MC2	PP2	19.6	21.7	40	2.3	110.9
MIDDLE finger								
Extensor Digitorum III+IV		Humerus	ExtWrap	41.9	286.2	0	9.9	223.8
Flexor Digitorum Superficialis III	5	Hum/Uln	MP3	65.0	240	15	9.7	141.2
Flexor Digitorum Profundus III	7	Ulna/ radius	DP3	59.4	290	0	12.3	196.0
Lumbricales 2FDPIII		FDP2/MC3	ExtWrap	73.7	0	0	1	12.8
Dorsal Interosseus 2	1	MC3/MC4	PP3	19.9	41	15	2.6	123.5
Dorsal Interosseus 3	1	MC2/MC3	PP3	16.9	36	25	2	112.2
RING finger								
Extensor Digitorum -IV	1	Humerus		51.6	306	0		0.0
Flexor Digitorum Superficialis IV(+V)	5	Hum/Uln	MP4	50.0*	260	0	5.8*	109.7
Flexor Digitorum Profundus IV(+V)	7	Ulna/ radius	DP4	54.7*	300	0	13.9*	240.5
Lumbricales III		FDPIV	ExtWrap	68.8	0	0	0.8	11.0
Palmar Interosseus III	1	MC4	PP4	20.9	10	19	1.3	58.9
Dorsal Interosseus IV	1	MC4/MC5	PP4	18.2	28	20	2.2	114.2
Little finger								
Extensor Digitorum-V	*x*	Not present		*x*	*x*	*x*	*x*	
Extensor Digiti Minimi	1	Humerus	ExtWrap	43.5	259	0	3.7	80.5
Extensor Digiti Minimi IV IV		Ulna	ExtWrap	45.7	133	0***	3.7***	0.0
Flexor Digitorum Superficialis IV+V	5	Ulna/ radius	MP5	50.0*	80		5.8*	
Flexor Digitorum Profundus IV+V	7	Ulna/ radius	DP5	54.7*	245		13.9*	
Opponens Digiti Minimi	0	MC3	MC5	16.7	36	0	2.3	130.2
Abductor Digiti Minimi	0	MC3	PP5	37.7	19.5	0	3.6	90.4
Lumbricales V		FDPV	PP5	61.1	0	0	0.5	7.7
Palmar Interosseus V	0	MC5	PP5	17.6	24.5	0	1.2	64.6
Flexor Digiti Minimi	0	MC3	PP5	33.6	6	0	0.4	11.3

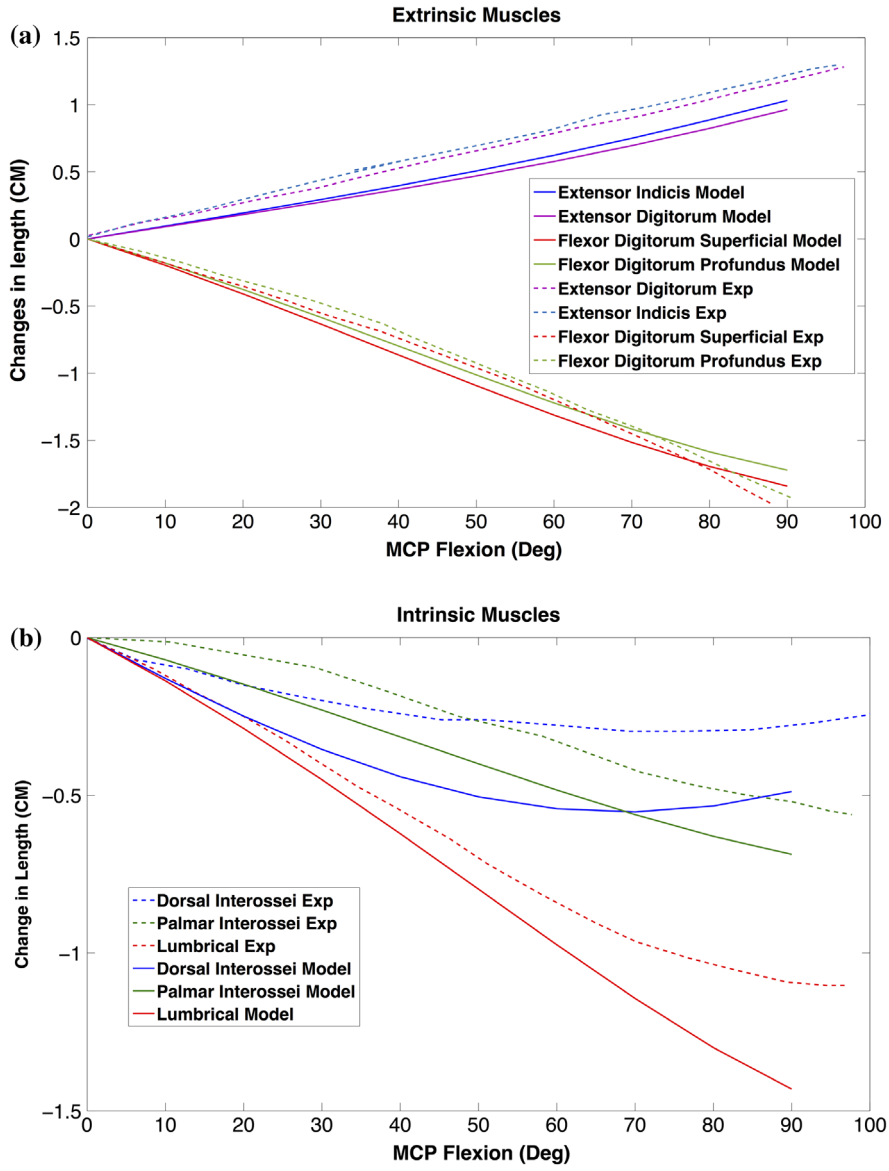

Figure 7. Changes in musculotendon length during flexion of index finger MCP acquired by model (solid lines). Experimental data (Exp – dashed lines) extracted from (An et al. 1983). (a) Extrinsic (b) Intrinsic.

collected data. In the dissection process no indication of a compromised musculoskeletal system arose. None of the MCP and PIP joints showed signs of osteoarthiris [no osteophytes or sclerosis]. To illustrate this, a selection of photographs of cadaver joints, are provided in the supplementary material. Furthermore this was supported by the kinematic data, which did not show indication of joint instability. Although we did not check indications of osteoporosis using DXA, there were no signs of osteoporosis.

Another simplification for acquiring details needed for modeling is that the muscle bellies of EDC, FDS, and FDP were dissected into separate muscle heads. This neglects the strong mechanical relationship between these head that can (at least partly) explain that fingers cannot fully move independently (Maas et al. 2003; Lang & Schieber 2004).However, these relationships may be considered in the model by subscribing activation constraints based on finger coupling patterns as observed in the previous studies (Zatsiorsky et al. 2000; Kim et al. 2008).

Differences in age, height, weight, and sex of subjects affect outputs of the model. As it was mentioned, anatomical data of the current study is obtained from an old female cadaver, therefore extrapolation of input data for other populations may have some difficulties depending on the desired accuracy. Using specific data-set for different range of population may be needed in order to examine if they can impose significant variations.

While the fact that the data-set collected in this study stems from one single specimen is one of the strong points of this study, application of the data in a musculoskeletal model to study a particular patient or subject may not suffice, since subject specific differences can introduce

important variations in functioning. In such cases, model scaling using subject-specific MRI or CT data may be useful. However, these should be used with caution as the validity of using such scaling methods is not known. Unfortunately for this specimen no MRI-data are available. It is advised, however, that future studies incorporate imaging data in the full data-set.

Conclusion

The presented data-set comprises geometrical and muscle contraction parameter data for the forearm and hand anatomy, collected on one single specimen. This complete and consistent data-set can serve as a basis for future musculoskeletal models of the hand and wrist. Such models can be used to obtain valuable insights in the general function of the musculoskeletal system of the wrist and hand or serve for example as a training tool for hand surgeons.

Disclosure statement

No potential conflict of interest was reported by the authors.

Funding

This project was partly funded by the European Commission through MOVE-AGE, an Erasmus Mundus Joint Doctorate program [2011-0015]. Huub Maas was partially supported by the Division for Earth and Life Sciences of The Netherlands Organization for Scientific Research [864-10-011].

References

An K, Ueba Y, Chao E, Cooney W, Linscheid R. 1983. Tendon excursion and moment arm of index finger muscles. J Biomech. 16:419–425.

An KN, Chao EY, Cooney WP 3rd, Linscheid RL. 1979. Normative model of human hand for biomechanical analysis. J Biomech. 12:775–788.

Borst, J., Forbes, P. A., Happee, R., Veeger, D. H. 2011. Muscle parameters for musculoskeletal modelling of the human neck. Clin Biomech (Bristol, Avon). 26:343–351.

Brook N, Mizrahi J, Shoham M, Dayan J. 1995. A biomechanical model of index finger dynamics. Med Eng Phys. 17:54–63.

Buford William L., Koh S, Andersen CR, Viegas SF. 2005. Analysis of intrinsic-extrinsic muscle function through interactive 3-dimensional kinematic simulation and cadaver studies. J Hand Surg. 30:1267–1275.

Chao EY, Opgrande JD, Axmear FE. 1976. Three-dimensional force analysis of finger joints in selected isometric hand functions. J Biomech. 9:387–396, IN2.

Friedman J, Flash T. 2009. Trajectory of the index finger during grasping. Exp Brain Res. 196:497–509.

Hill A. 1938. The heat of shortening and the dynamic constants of muscle. Proceedings of the Royal Society of London B: Biological Sciences. 126:136–195.

Holzbaur KRS, Delp SL, Murray WM. 2006. Moment-generating capacity of upper limb muscles. J Biomech. 39:S85–S85.

Holzbaur KR, Murray WM, Gold GE, Delp SL. 2007. Upper limb muscle volumes in adult subjects. J Biomech. 40:742–749.

Jacobson MD, Raab R, Fazeli BM, Abrams RA, Botte MJ, Lieber RL. 1992. Architectural design of the human intrinsic hand muscles. J Hand Surg Am. 17:804–809.

Kim SW, Shim JK, Zatsiorsky VM, Latash ML. 2008. Finger interdependence: Linking the kinetic and kinematic variables. Hum Mov Sci. 27:408–422.

Lang CE, Schieber MH. 2004. Human finger independence: limitations due to passive mechanical coupling versus active neuromuscular control. J Neurophysiol. 92:2802–2810.

Lee, J. H., Asakawa, D. S., Dennerlein, J. T., Jindrich, D. L. 2015. Finger muscle attachments for an OpenSim Upper-extremity model. PloS one. 10:e0121712.

Levangie, PK, Norkin, CC. 2011. Joint structure and function: a comprehensive analysis. Philadelphia (PA): FA Davis.

Maas H, Baan GC, Huijing PA, Yucesoy CA, Koopman BH, Grootenboer HJ. 2003. The relative position of EDL muscle affects the length of sarcomeres within muscle fibers: experimental results and finite-element modeling. J Biomech Eng. 125:745–753.

Nikooyan AA, Veeger HE, Chadwick EK, Praagman M, van der Helm FC. 2011. Development of a comprehensive musculoskeletal model of the shoulder and elbow. Med Biol Eng Comput. 49:1425–1435.

Sancho-Bru JL, Mora MC, León BE, Pérez-González A, Iserte JL, Morales A. 2014. Grasp modelling with a biomechanical model of the hand. Comput Method Biomech Biomed Eng. 17:297–310.

Sancho-Bru JL, Pérez-González A, Vergara-Monedero M, Giurintano D. 2001. A 3-D dynamic model of human finger for studying free movements. J Biomech. 34:1491–1500.

Söderkvist I, Wedin PA. 1993. Determining the movements of the skeleton using well-configured markers. J Biomech. 26:1473–1477.

Valero-Cuevas FJ, Johanson ME, Towles JD. 2003. Towards a realistic biomechanical model of the thumb: the choice of kinematic description may be more critical than the solution method or the variability/uncertainty of musculoskeletal parameters. J Biomech. 36:1019–1030.

Valero-Cuevas FJ, Towles JD, Hentz VR. 2000. Quantification of fingertip force reduction in the forefinger following simulated paralysis of extensor and intrinsic muscles. J Biomech. 33:1601–1609.

van der Helm FC. 1994. A finite element musculoskeletal model of the shoulder mechanism. J Biomech. 27:551–569.

Veeger HE, Yu B, An KN, Rozendal RH. 1997. Parameters for modeling the upper extremity. J Biomech. 30:647–652.

Vignais N, Marin F. 2014. Analysis of the musculoskeletal system of the hand and forearm during a cylinder grasping task. International Journal of Industrial Ergonomics. 44:535–543.

Vigouroux L, Domalain M, Berton E. 2009. Comparison of tendon tensions estimated from two biomechanical models of the thumb. J Biomech. 42:1772–1777.

Walker SM, Schrodt GR. 1974. I segment lengths and thin filament periods in skeletal muscle fibers of the rhesus monkey and the human. Anat Rec. 178:63–81.

Ward SR, Loren GJ, Lundberg S, Lieber RL. 2006. High stiffness of human digital flexor tendons is suited for precise finger positional control. J Neurophysiol. 96:2815–2818.

Wu JZ, An K-N, Cutlip RG, Andrew ME, Dong RG. 2009. Modeling of the muscle/tendon excursions and moment arms in the thumb using the commercial software anybody. J Biomech. 42:383–388.

Wu JZ, An KN, Cutlip RG, Dong RG. 2010. A practical biomechanical model of the index finger simulating the kinematics of the muscle/tendon excursions. Bio-Med Mater Eng. 20:89–97.

Zatsiorsky V, Seluyanov V, Chugunova L. 1990. Methods of determining mass-inertial characteristics of human body segments. Contemp Probl Biomech. 272–291.

Zatsiorsky VM, Li Z-M, Latash ML. 2000. Enslaving effects in multi-finger force production. Exp Brain Res. 131:187–195.